Spectrum Sensing in Cognitive Radio Using Multitaper Method Based on MIMO-OFDM Techniques

Ahmed O. Abdul Salam[1*], Ray E. Sheriff[1], Saleh R. Al-Araji[2†], Kahtan Mezher[2], Qassim Nasir[3]

1. School of Engineering and Informatics, University of Bradford, Bradford, BD7 1DP, UK
2 . († formerly) College of Engineering, Khalifa University for Science and Technology, P.O. Box 127788, Abu Dhabi, UAE
3. College of Engineering, University of Sharjah, Sharjah, UAE

* Corresponding author, Email: aoa_salam@yahoo.com

***Abstract*—The current inefficient utilization of frequency spectrum has alerted regulatory bodies to streamline improvements. Cognitive radio (CR) has recently received considerable attention and is widely perceived as a promising improvement tool in estimating, or equivalently sensing, the frequency spectrum for wireless communication systems. The cognitive cycle in CR systems is capable of recognizing and processing better spectrum estimation (SE) and hence promotes the efficiency of spectrum utilization. Among different SE methods, the multi-taper method (MTM) shows encouraging results. Further performance improvement in the SE for CR can be achieved by applying multiple antennas and combining techniques. This paper proposes a constructive development of SE using MTM, abbreviated as MTSE, and by employing multiple-input multiple-output (MIMO), parsed into separate parallel channels using singular value decomposition (SVD), and maximum ratio combining (MRC) configurations. Deviating from these improvements, however, multicarrier systems such as orthogonal frequency division multiplexing (OFDM) show inferior sensing performances due to the noise multiplicity generated and combined from all subcarrier channels. By means of the quadrature matrix form, the probabilities for such integrated settings of SE have been derived to reach at their approximate asymptotes. Numerical simulations revealed specific better performances stemmed from coupling the fashionable MTSE and MIMO technologies.**

***Index Terms*— Cognitive radio, spectrum estimation, multi-taper, multiple-input multiple-output, orthogonal frequency division multiplexing, singular value decomposition**

I. Introduction

Further to scarcity of the radio frequency spectrum, recent studies have pointed to the detrimental management caused by stagnant and inflexible rules and policies currently governing this prime natural asset [1-7], and references therein. The term "white holes or spaces" has been commonly used to label empty or rarely utilized frequency spectrum segments in wireless communication systems. Such white holes are usually reserved for licensed primary users (PU) and, hence, their utilization would be highly determined by their communication activities and habits. Such an uncontrolled scheme of precious air link resources would render certain spectrum bands below their proper quality of service (QoS) levels. This also generates burdens for opportunistic secondary users (SU) to fill in these unused frequency spaces when not engaged by PUs. Such adverse situations are largely attributed to degraded management habits imposed by various authorities and commercial business partners sharing the services control offered to vast customers over these frequency bands and channels. Therefore, and as pioneering initiatives, both the Federal Communications Commission (FCC) in the USA and the Electronic Communications Committee (ECC) in Europe have recently standardized the spectrum reutilization in the TV band, which is called TV white space (TVWS). The idea of TVWS recycling is generally considered as very attractive due to its low utilization and good propagation properties [1].

The term cognitive radio (CR) is inspired to promote sustainable solutions for crucially challenging spectrum issues. The CR system, based on software defined radio (SDR), is considered as a versatile smart platform that is aware of its surroundings and reacts accordingly. The reaction is interpreted in terms of frequency spectrum and modulation features, power and rate, and adapts the transmission parameters accordingly [5, 6]. It is projected that CR systems will rely heavily on current wireless communication platforms with more intelligence ingredients added to allow for better collaboration and coordination among multiple systems of service providers and end users.

Surveys on spectrum estimation (SE), or equivalently with decision making called spectrum sensing (SS), in wireless systems are proliferated in the literature [1-4, 7]. In the broader context, SE techniques can be generally premised on either narrowband or wideband regimes. Different work environments determine the type of SE, which generally can be categorized under three main groups: 1) guided where both signal and noise information required such as likelihood ratio test (LRT), matched filter (MF), and cyclostationary detection (CD); 2) semi-guided or semi-blind where only noise information is required, such as energy detection (ED) and wavelet-based sensing, and; 3) unguided or blind that requires no information on signal or noise, such as emerging maximum

to minimum eigenvalue (MME), covariance (COV) and blindly combined ED detections. Alternative schemes using the multi-taper method (MTM) have recently attracted more attention for SE in recent literature [5-14]. The MTM is rooted to a particular type of discrete prolate spheroidal (DPSS) tapers named after Slepian. Such tapers use orthogonal data sets to trade-off between spectral estimate resolution and variance without compromising bias effects. The MTM for SE has therefore been highly advocated for its robust energy control within the desirable bands, and reduced the undesirable out-of-band (OOB) spectrum leakage. Robust SE paradigms are decisive for efficient and sustainable spectrum utilization, and hence the design of which must be handled with a paramount care.

Recent studies demonstrated that multiple-input multiple-output (MIMO) and orthogonal frequency division multiplexing (OFDM) are widely accepted as key enabling technologies in CR systems [15-18]. The merger between MIMO and OFDM promises the fulfilment of challenges set forward by next-generation demanding trend of very high speed and reliable wireless communication systems. The MIMO deployment enhances transmission speed and capacity to the highest plausible limits; however, system complexity might be implied. Irrespective of that, the lower data rate places on each antenna compared to the original, offsets such complication. Moreover, MIMO platforms do not demand considerable increase in the transmission power. Furthermore, spatial diversity techniques are essential for signal reproduction on the receiver's side. Since it maximizes the signal-to-noise ratio (SNR) at the receiver output, the maximum ratio combining (MRC) is considered as optimum among other diversity techniques. This is credited to the output SNR summing SNRs from all receive antennas and achieving full diversity under various conditions [19-21]. From another perspective, typical wireless channels suffer severe multipath fading effects. Among several recent studies in this regard, one particularly interesting investigation [22] showed that fading, such as Nakagami type, can cause harmful correlation between channels and this will degrade the detection process. Therefore, a mitigation approach employing diversity techniques, especially MRC, was suggested to alleviate such fading effects and eventually render the SE performance more robust against noise uncertainty [13, 22]. An alternative remedy of fading is by exploiting multicarrier (MC) or multitoned (MT) transmission features. Hence, OFDM lends itself as realistic representation of a time-limited MC scheme mainly intended to combat channels' defects.

A. *Contributions*

Motivated by the virtuous impact of MIMO-OFDM techniques, this work appraises the features of MTM, MRC and MRT as promising substance for SE in CR systems. The core objective is to detect a PU presence by interrogating the spectrum signature throughout the entire licensed channels, and not over individual sub-channels or subcarriers. An instructive approach for deriving signal models and performance measures will also be explored. The context assumes additive white Gaussian noise (AWGN), uncorrelated flat fading channels, no transmission guard prefixes, and without collaboration on spectrum accessibility.

The most notable contributions of this paper can hence be summarized as follows

- Systematic modelling of the MIMO-OFDM procedures that are central to the design and analysis of the proposed MTSE algorithm.
- Employ the SVD, equipped with the MRC, to perform the MIMO-OFDM eigen-channel decomposition to render the application of MTSE tractable.
- Apply the quadrature matrix form to approximate the MTSE using MIMO-OFDM scheme, with the aim of improving the SE under low SNR regimes.
- Develop the close-form expressions for the MTSE-MIMO and OFDM optimal detection statistics in the framework of Neyman-Pearson (NP) hypothesis test.
- Demonstrate the desirable performance of the MTSE-MIMO in comparison with the traditional PSE approach.
- Recognize the poor performance of the given SE algorithms under different OFDM carrier settings.
- Illustrate the sufficient number of Slepian tapers and assess the extent of their effect on the SE detection.

B. *Outline*

The remainder of this paper is organized as follows. Section 2 introduces the system build-up, and Section 3 presents the basic MIMO-OFDM. Section 4 is on the analysis of MTSE, while Section 5 is on the statistical detection. Numerical results are provided in Section 6, followed by the concluding remarks.

II. System Architecture

The proposed conceptual architecture of a baseband CR system employing MIMO-OFDM, MRC and MTM components is shown in Fig. 1.

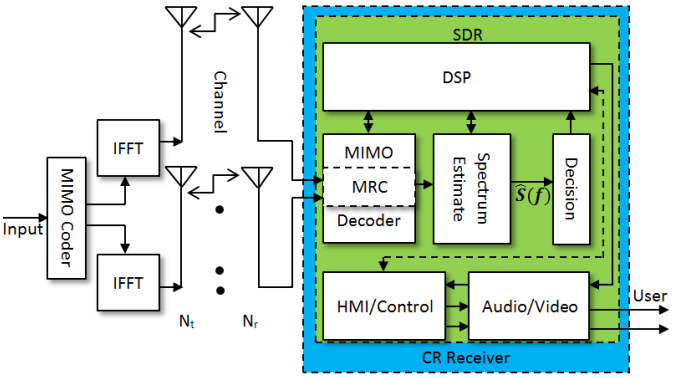

Fig. 1. Simplified diagram of SS based on MIMO-OFDM in CR receiver.

The radio and intermediate frequency (RF and IF) stages are omitted for clarity and simplicity of presentation. The intelligence of CR is credited to the presence of SDR. The SDR constitutes all necessary digital signal processing (DSP) to perform the various intended tasks, such as: SE, automatic modulation classification (AMC), interference removal, channel equalization, adaptation, spatiotemporal decoding,

memory storage, etc. While the SDR resembles the physical layer in equivalent operating systems (OS), the main control functions including entire OS layers, human machine interface (HMI) and other audio and video boards are inherited by the CR. The favorable performance of a post-detection combining strategy is adopted here, given the co-phasing is well managed.

III. Problem Statement

In the analysis presented in this section, matrices are denoted by bold capital letters, vectors by bold small and capital letters, while scalars by normal small and capital letters.

A. Basic OFDM

Consider an OFDM scheme where a block of K data symbols is transmitted in parallel on N_c subcarriers. The time duration of an OFDM symbol is K times larger than that of a single-carrier (SC) system. The cyclic prefix (CP) and cyclic suffix (CS) augmented guard samples are not considered in this analysis. The OFDM transmission system can be effectively realized in discrete time by employing an inverse fast Fourier transform (IFFT) to act as a modulator and an FFT to act as a demodulator. The transmitted data are the "frequency" domain coefficients, and the samples at the output of the IFFT stage are "time" domain samples of the transmitted sequence. Suppose there is a K-length data symbol block of the form $X = \{X(0), X(1), \dots, X(K-1)\}$. Applying the IFFT on this data block will generate the time domain sequence $x = \{x(0), x(1), \dots, x(K-1)\}$ represented by [15, 16, 20, 21]

$$\{x(k)\} = \text{IFFT}_{N_c}\{X(k)\} \tag{1}$$

The input data sequence $x(k)$, with $\text{E}|x(k)|^2 = \sigma_x^2$, is modulated by a particular M-ary constellation mapping process, such as M-ary phase shift keying (MPSK) or M-ary quadrature amplitude modulation (MQAM), resulting in the complex symbol stream $X(k)$. It is important to note that IFFT and FFT must have equal number of points in time and frequency domains, that is $K = N_c$, which are bigger than the M-ary number of symbols.

B. MIMO Configuration

Consider the scenario of a base station (BS), equipped with N_t transmitting antennas, and with designated links to mobile stations (MS) or PUs. There are also SUs, provided with N_r receiving antennas, roaming in the same topographical landscape and hungry for opportunistic utilization of non-maintained links, or empty channels. The link transmission is taking place using OFDM with N_c subcarriers arranged in a MIMO configuration over a slowly varying frequency-selective channel. The complex baseband received sequence over one path and $n_c = \{0, 1, \dots, N_c\}$ subcarrier is denoted by [15, 16, 20, 23]

$$y_{n_r,n_c} = \sum_{n_t=0}^{N_t} h_{n_r,n_t,n_c}\, x_{n_t,n_c} + w_{n_r,n_c} \tag{2}$$

where the time attribute omitted in the second expression for simplicity. Revising in matrix form to consider all channel paths we get

$$\boldsymbol{y}_{n_c} = \boldsymbol{H}_{n_c} x_{n_c} + \boldsymbol{w}_{n_c} \tag{3}$$

where $\boldsymbol{H}_{n_c}$ is $N_r \times N_t$ the quasi-static frequency response channel matrix denoted by $n_t = \{0, 1, \dots, N_t\}$ traversing $n_r = \{0, 1, \dots, N_r\}$ paths, $\boldsymbol{w}_{n_c}$ is AWGN with $\mathcal{CN} \sim (0, \sigma_w^2 \mathbf{I})$, and $\mathbf{I}$ is an identity matrix and all, including $\boldsymbol{y}_{n_c}$, can be viewed as variables colligated over channel paths.

C. SVD Channel Representation

The SVD disintegrates a MIMO channel matrix to produce independent parallel paths collimated in the direction of a receiver. The SVD representation of a channel is given by $\boldsymbol{H}_{n_c} = \boldsymbol{U}_{n_c} \boldsymbol{\Sigma}_{n_c} \boldsymbol{V}_{n_c}^{\text{H}}$, where $\boldsymbol{U}_{n_c}$ and $\boldsymbol{V}_{n_c}^{\text{H}}$ are orthonormal left and right singular vectors, respectively, $\boldsymbol{\Sigma}_{n_c}$ is a diagonal matrix whose entries are nonnegative singular eigenvalues arranged from largest to smallest, and $(.)^{\text{H}}$ is the Hermitian operator. Equation (3) can hence be revisited as follows [15, 16, 20, 21]

$$\boldsymbol{y}_{n_c} = \boldsymbol{\Sigma}_{n_c} \widetilde{\boldsymbol{x}}_{n_c} + \widetilde{\boldsymbol{w}}_{n_c} \tag{4}$$

A pre-code processing is carried out on the transmitter side by multiplying the data sequence by $\boldsymbol{V}_{n_c}$ to generate $\widetilde{\boldsymbol{x}}_{n_c}$, while post-code processing is applied on the receiver side by multiplying the received sequence and noise by $\boldsymbol{U}_{n_c}^{\text{H}}$ to generate the original data sequence and modified noise variable $\widetilde{\boldsymbol{w}}_{n_c}$. Such post processing will not change the statistical characteristics of the involved sequences since $\boldsymbol{U}_{n_c}^{\text{H}}$ has unitary entries. Accordingly, a tone-by-tone MIMO-OFDM system can transform a frequency-selective MIMO channel into a collection of $N_c \times R$ parallel frequency-flat sub-channels, where $R = \min\{N_t, N_r\}$ is the minimum number of antennas at each end. Assume $r = \{1, 2, \dots, R\}$ and availing the SVD, revises (4) to be

$$\boldsymbol{y}_{n_c} = \begin{bmatrix} g_1 & 0 & \cdots & 0 \\ 0 & \ddots & \cdots & 0 \\ \vdots & \vdots & g_R & \vdots \\ 0 & 0 & \cdots & 0 \end{bmatrix}_{n_c} \widetilde{\boldsymbol{x}}_{n_c} + \widetilde{\boldsymbol{w}}_{n_c} \tag{5}$$

where the SVD matrix $\boldsymbol{\Sigma}_{n_c}$ is of size $N_r \times N_t$ and rank R decomposition of the channel matrix over N_c frequency bins, $g_r = \sqrt{\lambda_r}$ is the gain of each parallel channel, or the square root of r^{th} eigenvalue of $\boldsymbol{H}\boldsymbol{H}^{\text{H}}$. The received signal elements are hence decoupled and can be processed separately since they are identical and independent distribution (i.i.d.) statistical processes. The size of $\boldsymbol{U}_{n_c}$ and $\boldsymbol{V}_{n_c}^{\text{H}}$ is $N_r \times N_r$ and $N_t \times N_t$, respectively, and both are dimensioned to N_c bins.

D. MRC Processing

The MRC is selected among other popular linear combining techniques aimed at improving a fading channel's reception. The treatment of linear combining is of special interest due to

its straightforward implementation and tractable performance analysis in terms of mathematical construction. The realization of MRC is based on the assumption that the channel parameters are either perfectly known or estimated. Let us first consider the MRC performance under full-order diversity applied to all N_c subcarriers. Using a linear combining vector $\boldsymbol{a}$ with coefficients $[a_1, a_2, \dots, a_R, .0]^{\mathrm{T}}$ of size N_r, and $(.)^{\mathrm{T}}$ is the transpose operator, the combined estimated output for a single frequency bin can be of the following variable form

$$y_{n_c} = \boldsymbol{a}_{n_c}^{H} \begin{bmatrix} g_1 & 0 & \cdots & 0 \\ 0 & \ddots & \cdots & 0 \\ \vdots & \vdots & g_R & \vdots \\ 0 & 0 & \cdots & 0 \end{bmatrix}_{n_c} \widetilde{\boldsymbol{x}}_{n_c} + \boldsymbol{a}_{n_c}^{H} \widetilde{\boldsymbol{w}}_{n_c} \tag{6}$$

and by summing over all subcarriers yields

$$y = \sum_{n_c=0}^{N_c-1} \left\{ \boldsymbol{a}_{n_c}^{\mathrm{H}} \begin{bmatrix} g_1 & 0 & \cdots & 0 \\ 0 & \ddots & \cdots & 0 \\ \vdots & \vdots & g_R & \vdots \\ 0 & 0 & \cdots & 0 \end{bmatrix}_{n_c} \widetilde{\boldsymbol{x}}_{n_c} + \boldsymbol{a}_{n_c}^{\mathrm{H}} \widetilde{\boldsymbol{w}}_{n_c} \right\} \tag{7}$$

Now, the MRC acts as a spatial-temporal matched filtering (STMF) in order to extract a maximal amount of information from the multiple received signals [19-21]. In receive STMF, or MRC, this would stipulate phase alignment among all received signals to add up constructively as per the larger weight assigned to stronger channels. Since we have broken down the multipath channel indexes into parallel virtual receive channels, then the MRC weighting factors must coherently match with the gain eigenvalue of each channel. This can only be achieved if $a_r = g_r^*$, where $(.)^*$ is the conjugate operator [19, 20]. For Hermitian channels the entries for $\boldsymbol{\Sigma}_{n_c}$are all positive real values, hence (7) can be written as

$$y = \sum_{n_c=0}^{N_c-1} \left\{ \begin{bmatrix} \lambda_1 & 0 & \cdots & 0 \\ 0 & \ddots & \cdots & 0 \\ \vdots & \vdots & \lambda_R & \vdots \\ 0 & 0 & \cdots & 0 \end{bmatrix}_{n_c} \widetilde{\boldsymbol{x}}_{n_c} + \boldsymbol{a}_{\boldsymbol{n_c}}^{\mathrm{H}} \widetilde{\boldsymbol{w}}_{n_c} \right\} \tag{8}$$

Assume $\widetilde{\boldsymbol{\Sigma}}_{n_c} = \mathrm{diag}[\lambda_1, \lambda_2, \dots, \lambda_R, \dots, 0]$, and since the noise statistical characteristics will remain intact after all mathematical manipulations [18-20], (8) is rewritten as

$$y = \sum_{n_c=0}^{N_c-1} \left\{ \widetilde{\boldsymbol{\Sigma}}_{n_c} \widetilde{\boldsymbol{x}}_{n_c} + \widetilde{\boldsymbol{w}}_{n_c} \right\} \tag{9}$$

IV. MTM Spectrum Estimation

The MTM spectral estimate (MTSE) uses a special window of varying length to control the bias-variance trade-offs. The Slepian tapers are commonly employed in such windowing applications for their having a robust control on spectral leakage deficiencies. Such tapers relate to data sequences of a given length K with maximal spectral concentrations in a specified bandwidth, B. Solving the following Toeplitz matrix eigenvalue equation produces tapers [9-10]

$$\boldsymbol{R}\boldsymbol{v}_k = \psi_k \boldsymbol{v}_k \tag{10}$$

where $\boldsymbol{R}$ is the $K \times K$ positive-definite Toeplitz autocorrelation matrix and the $(p, q)^{\text{th}}$ entry of this kernel matrix is defined by

$$R_{p,q} = \frac{\sin 2\pi B(p-q)}{\pi(p-q)} \quad , \quad p, q = 1, 2, \dots, K \tag{11}$$

and the tapers, or principle eigenvalues ψ_k of the eigenvector $\boldsymbol{v}_k$, are ranged between 0 and 1 and organized in a descending order such that $\psi_0 \geq \psi_1 \geq \cdots \geq \psi_{K-1}$. The first $L \approx 2KB$ of these tapers are dominating, i.e., their values are close to 1, whereas the rest are of negligible effect. Moreover, the tapers of lower order have capability for much stronger power concentration than their higher order counterparts, suggesting that it suffices to use the first L tapers for spectral estimation. The range between 3-to-6 [8], or 2-to-8 [5, 6, 10] is reasonable for the dominant tapers. The parameter choice of time-bandwidth product KB is a tradeoff between spectral resolution and variance, where the time sample size K is assumed equivalent to the FFT sensing frame, and B is the bandwidth normalized by the sample rate.

The power spectral density (PSD) estimate is the sum of weighted eigenspectrums of tapered data sequence in the frequency domain [5-14] is given by

$$\hat{S}_y(f) = \frac{\sum_{l=0}^{L-1} \psi_l |Y_l(f)|^2}{\sum_{l=0}^{L-1} \psi_l} = \sum_{l=0}^{L-1} \alpha_l \, |Y_l(f)|^2 \tag{12}$$

and for a finite sample-size constraint, the power distribution of each eigenspectrum falls between the bandwidth from $f - B$ to $f + B$. The FFT of the received data sequence for particular Slepian tapers $\{v_l\}_{k=0}^{K-1}$ is

$$Y_l(f) = \frac{1}{K} \sum_{k=0}^{K-1} y(k) v_l(k) e^{-j2\pi fk} \tag{13}$$

The weighting factors $\alpha_l = \psi_l / (\psi_0 + \cdots + \psi_{L-1})$ represent another set of eigenvalues associated with each of the l^{th} eigenspectrum. The normalization factor $\sum_{l=0}^{L-1} \psi_l$ can be ignored since its totality equals 1, without impact on the decision policy. Parseval's theorem for total power entails adding and averaging of all tapers and dominant channel eigenvalues for each FFT bin. Hence, fill into (12) and (13) for (9) yields the scalar expressions realized over r parallel paths

$$Y_{n_c,l}(f) = \frac{1}{RK} \sum_{r=1}^{R} \sum_{k=0}^{K-1} y_{r,n_c}(k) v_l(k) e^{-j2\pi fk} \tag{14}$$

$$\hat{S}_{y,n_c}(f) = \frac{1}{RLK} \sum_{l=0}^{R} \sum_{l=1}^{L} \sum_{k=0}^{K-1} \alpha_l \left| y_{r,n_c}(k) v_l(k) e^{-j2\pi fk} \right|^2 \tag{15}$$

To simplify the illustration exposition, the above equations can be put in a quadratic matrix form suitable for decision

statistics. Therefore, the following forms are proposed as a modified extension to [8-10, 12]

$$\begin{aligned} \boldsymbol{v}_l &= [v_l(1), v_l(2), \dots, v_l(K)]^T \\ \boldsymbol{y}_{r,nc} &= \left[y_{r,n_c}(1), y_{r,n_c}(2), \dots, y_{r,n_c}(K)\right]^T \\ \mathbf{a} &= [e^{j2\pi f}, e^{j2\pi f 2}, \dots, e^{j2\pi f K}]^{\mathrm{T}} \end{aligned} \tag{16}$$

and $\boldsymbol{b}_l = \boldsymbol{v}_l \odot \boldsymbol{a}$ where $\odot$ refers to the Hadamard product. Substituting (16) in (13) reveals $Y_{n_c,l}(f) = \boldsymbol{b}_l^H y_{n_c}$, and when used together with the Slepian tapers alters (12) to have the following spectral estimate

$$\hat{S}_{y,n_c}(f) = \frac{1}{RLK}\sum_{r=1}^{R} \boldsymbol{y}_{r,nc}{}^H \boldsymbol{\Omega} \boldsymbol{y}_{r,nc} \tag{17}$$

where $\boldsymbol{\Omega}$ is $L \times L$ idempotent matrix defined as $\boldsymbol{\Omega} = \sum_{l=0}^{L-1} \alpha_l \mathbf{b}_l \mathbf{b}_l^{\mathrm{H}}$. The above scalar PSD expression can be viewed as the totality of individual PSDs retrieved from the prevailing tapers' branches over all decomposed individual channels.

V. Decision Statistics

The binary hypotheses test (BHT) will be employed as a statistical tool to attain a decision on the SE outcome. The BHT will constitute $\mathcal{H}_0$ to denote the idle state of the PU; $\mathcal{H}_1$ represents the active state of the PU. To classify the observations into $\mathcal{H}_0$ or $\mathcal{H}_1$, a sufficient test statistics Λ is formulated, and for some threshold value η the general test decision is to contemplate $\mathcal{H}_0$ if $\Lambda \leq \eta$ otherwise $\mathcal{H}_1$ if $\Lambda > \eta$. The conditional probability distribution function (PDF) of such a BHT procedure is illustrated in Fig. 2 below. The bell shape statistical approximation is valid given the assumption of large number theory.

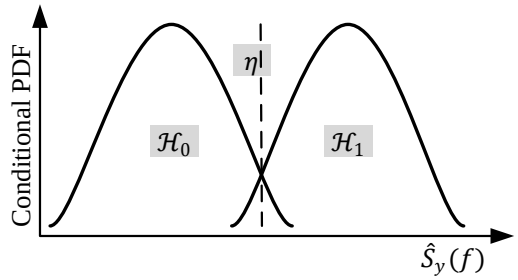

Fig. 2. PDF of BHT process.

The general task of a non-parametric SE is for the receiver to correctly detect the PU presence given only the received samples of processed eigenspectra $\hat{S}_y(f)$, while being uninformed about the symbols $\boldsymbol{X}$, the channel $\boldsymbol{H}$ and the noise power σ_w^2. Two pertinent probabilities are to be distinctive: 1) the probability of detection P_D, which is the probability that the PU channel is correctly detected by the SU while the BS in its active mode, and; 2) the probability of false alarm P_{FA}, which represents the probability of a false detection of the PU when it is in the idle state, i.e., no transmission from the BS on the PU particular channel. Given the sufficient test Λ defined in terms of $\hat{S}_y(f)$, then the probabilities in the framework of Neyman-Pearson (NP) optimal criterion are given below for one bin of the entire carriers

$$\begin{aligned} P_{FA}(bin) &= \Pr\{\hat{S}_{y,nc}(f) > \eta | \mathcal{H}_0\} \\ P_D(bin) &= \Pr\{\hat{S}_{y,nc}(f) > \eta | \mathcal{H}_1\} \end{aligned} \tag{18}$$

where η is an appropriate threshold value to maintain a constant false alarm rate (CFAR). The CFAR is commonly used in thresholding necessary values for spectrum estimators.

To examine the distribution of the random vector $\hat{S}_{y,nc}(f)$ under both hypotheses, it is useful to invoke the partial test statistics, briefly (PTS), denoted as Λ_{r,n_c}. Such a PTS expression was manifested on ED algorithm in some recent studies [23, 24], and it is also believed here that it resembles the local MTM-SVD approach given elsewhere [14]. So much as that and for one plausible interpretation, we can imagine the situation of having R separate channel paths and each is loaded with K samples of i.i.d. complex circular Gaussian noise with zero mean and σ_w^2 variance. Then each taper branch will convert each sample into central Chi-square variable χ^2 and summing over L tapers resulting in χ_{LK}^2 of LK degree of freedom, which is assigned for each individual Λ_{r,n_c}. Then, and in a similar approach to [24], but approximated for the sum of channel eigenvalues to 1 and ignoring all irrelevant constants, the above BHT can be realized as

$$\begin{aligned} &\text{Decide: } \mathcal{H}_0 \text{ if } \hat{S}_{y,nc}(f) \approx^{\mathrm{d}} \sigma_w^2 \chi_{RLK}^2 \\ &\text{Decide: } \mathcal{H}_1 \text{ if } \hat{S}_{y,nc}(f) \approx^{\mathrm{d}} (\sigma_x^2 + \sigma_w^2)\chi_{RLK}^2 \end{aligned} \tag{19}$$

where $\approx^{\mathrm{d}}$ stands for "equal in distribution". The probabilities can hence be further simplified assuming we have a large combination number of processed random sequences and channels. On this basis, or equivalently the central-limit theory, the approximations given in [25, 26] can be altered to

$$P_{FA}(bin) = \mathrm{Q}\left\{\frac{\eta - RLK\sigma_w^2}{2\sigma_w^2\sqrt{RLK/2}}\right\} \tag{20}$$

$$P_D(bin) = \mathrm{Q}\left\{\frac{\eta - RLK(\sigma_x^2 + \sigma_w^2)}{2(\sigma_x^2 + \sigma_w^2)\sqrt{RLK/2}}\right\} \tag{21}$$

where $\mathrm{Q}(.)$ is the right tail cumulative distribution function.

Let us now consider the effect of the entire frequency bins on the probabilities as given above for each individual bin. For such situation, the problem can be reduced to the detection of an unknown phase or frequency signal [27], where the total P_{FA} easily lends itself to have the following form

$$P_{FA} = N_c P_{FA}(bin) = N_c \mathrm{Q}\left\{\frac{\eta - RLK\sigma_w^2}{2\sigma_w^2\sqrt{RLK/2}}\right\} \tag{22}$$

and the total P_D can be easily deduced as given below

$$P_D = \mathrm{Q}\left\{\left(\frac{1}{(\mathrm{SNR}+1)}\right)\mathrm{Q}^{-1}\left(\frac{P_{FA}}{N_c}\right) - \sqrt{\frac{RLK}{2}\mathrm{SNR}}\right\} \quad (23)$$

where $\mathrm{SNR} = \sigma_x^2/\sigma_w^2$. It is evident that P_{FA} increases about linearly with respect to the number of bins examined, which means further performance degradation as the OFDM order increases. The P_D can easily aspire the SNR of binary symbols γ_b at the source in terms of the SNR of M-ary constellation γ_s, which is governed by $\gamma_s = \gamma_b \log_2 M$ [21], and hence yields

$$P_D = \mathrm{Q}\left\{\left(\frac{1}{(\log_2 M\gamma_b + 1)}\right)\mathrm{Q}^{-1}\left(\frac{P_{FA}}{N_c}\right) - \sqrt{\frac{RLK}{2}\gamma_b \log_2 M}\right\} \quad (24)$$

The statistics applied over the entire bins package are aimed to represent a particular channel of interest that can either be empty or occupied by PUs. Such application is typically known as a wideband or multiband SE, which is different than an individual band or sub-channel SE associated to each bin or carrier frequency commonly encountered in the literature [28, 29]. This paper uses one BHT procedure for a given group of sub-bands, or alternatively sub-channels, entered around arbitrary OFDM subcarriers. The proposed MTSE hence operates over the total frequency bands simultaneously rather than a single band each time, which allows the CR to perform local detection for a group of the sub-bands using only one detection procedure instead of multiple detections. This is in agreement with [30, 31], as all sub-bands in a group are usually expected to have a common status indicator about the presence or the absence of PUs.

Furthermore, this paper employs the pre-combining detection scheme where the signals received from multiple antennas are combined using the MRC technique before processing with the SE. Such an approach has been found to be more efficient in terms of computational complexity and yields consistent improvement in the detector performance, as suggested in [32], and also portrayed in [13, Fig. 1] .

VI. Numerical Results

The proposed MTSE scheme is numerically evaluated for performance corroboration. Let the choice of the appropriately sufficient number of Slepian tapers be discussed first. The Slepian taper representation is given in Fig. 3 using half time-bandwidth product KB equal to 0.125 and 1, respectively, while the energy contents of which are depicted in Fig. 4.

It is evident from Fig. 4 that the increase in the number of tapers would not be beneficial to the MTSE algorithm as the most energy is actually concentrated in the tapers of low order. These lower order tapers impose higher control on the spectrum bias, and the converse is true for the higher order tapers. It becomes obvious that the performance of the Slepian tapers act as a low pass filter, as per formulae (10 and 11) given above, and hence provide sharp spectrum truncation and better smoothing. Increasing the number of tapers will have energy spilled over many orthogonal elements. As the KB increases from 0.125 to 1, the tapers behavior becomes more erratic as more energy is now jumping to the tapers of higher order. Hence, the number of effective tapers might need to be slightly increased to retain some of the escaping energy to adjacent higher tapers. The higher the number of tapers, the more processing burdens unnecessarily invoked and, hence, practically meaningful values need to be managed.

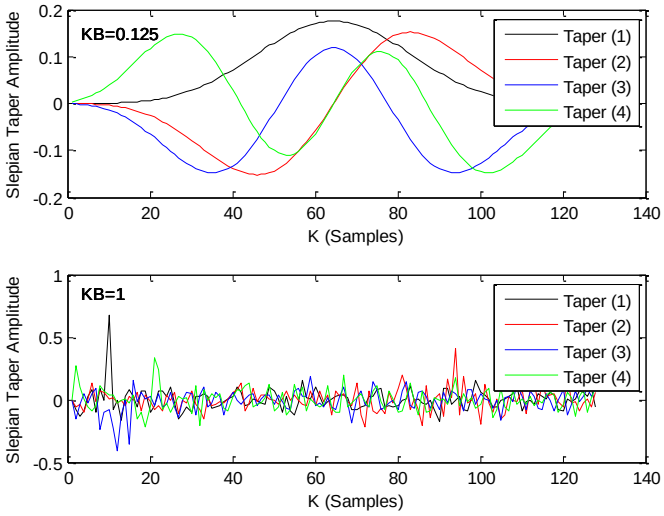

Fig. 3. Representation of 4 Slepian tapers with two different KB.

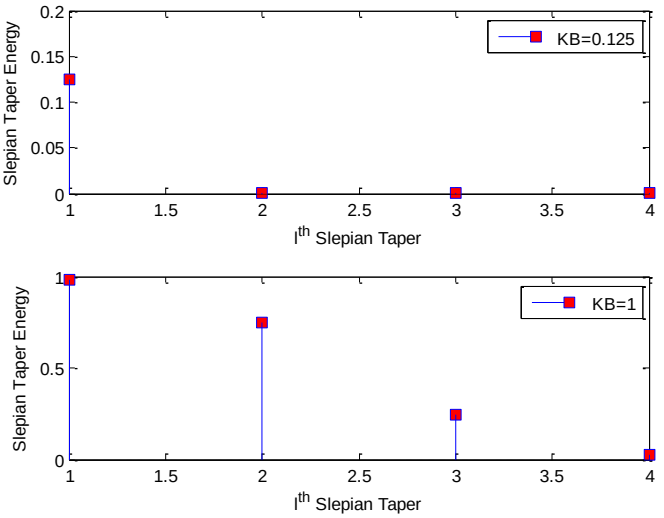

Fig. 4. Energy content of 4 Slepian Tapers with two different KB.

One of the essential evaluation tools is the receiver operation characteristic (ROC) curve, which governs the two probabilities given in (22) and (24). Since the ROC curve shows the achieved P_D as a function of the P_{FA}, it exposes the general performance for a particular detector. The sum of P_D and P_{FA} values at any point on this ROC performance graph is equal to 1. Aiming at computational ease and having clear graphics as far as possible, two dominant tapers are used with 1 and 2 parallel paths channel, respectively. The M-ary size has been intentionally fixed to $M = 2$ to manifest the case of

binary PSK (BPSK). The number of subcarriers varied from 16 to 64 and for several data symbols and the range of subcarriers equals the FFT order in this case. Fig. 5 illustrates the first ROC exercise employing 2 tapers. As expected, the ROC experiences a better trend when the number of dominant channels is increased. However, an adversary performance is obvious with respect to increasing the FFT order. The larger the FFT order, the worse performance is obtained.

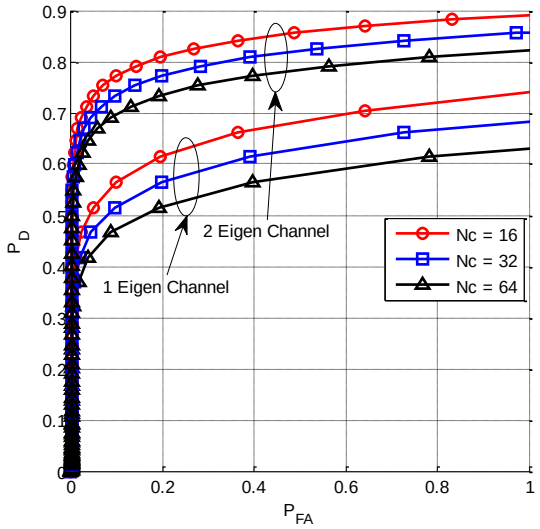

Fig. 5. ROC of MTSE with 2 tapers and MIMO-OFDM versus different FFT and channel orders.

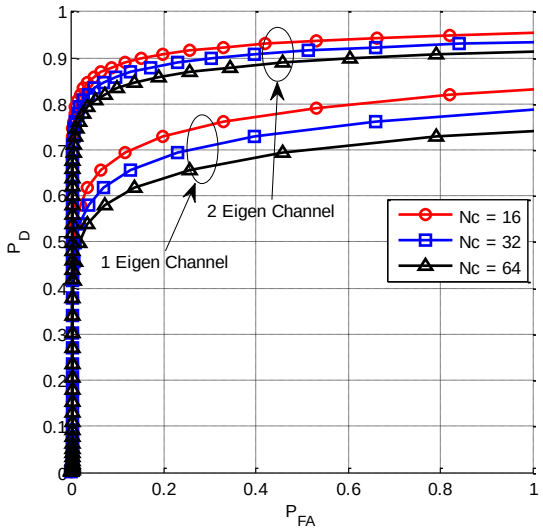

Fig. 6 ROC of MTSE with 3 tapers and MIMO-OFDM versus different FFT and channel orders.

Further noticeable enhancement in the ROC graph can also be gained when the number of tapers is increased to 3 as shown in Fig. 6. The above was repeated to consider the case of having different M-ary settings varied within the range of 2, 4, and 8, while keeping the FFT order or subcarrier to 16 as shown in Fig. 7 below. Such M-ary order may resemble the case of having BPSK, 4-PSK or QAM, and 8-PSK or 8-QAM, respectively. It is quite evident the gain realized in the detector performance, while increasing the number of M-ary order. The higher the M-ary order, the more power possessed in the complex symbols and hence the better performance achieved.

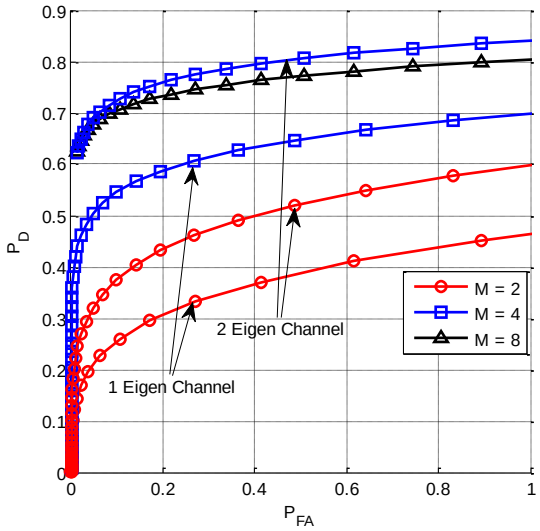

Fig. 7. ROC of MTSE with 2 tapers and MIMO-OFDM versus different M-ary and channels order.

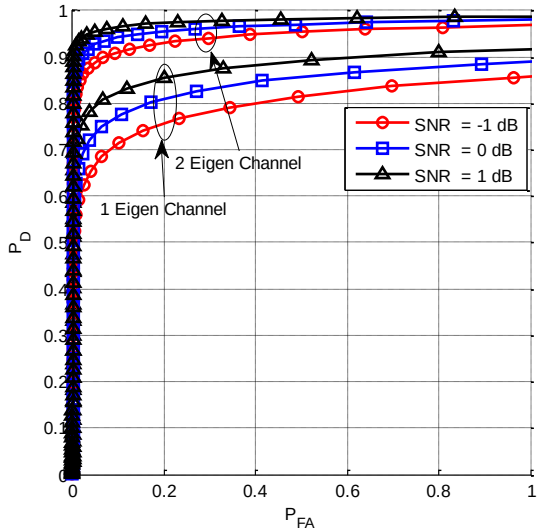

Fig. 8 ROC of MTSE with 2 tapers and MIMO-OFDM versus SNR variations.

Additional key assessment is by plotting the ROC performance against the SNR variations. Such a chart is depicted in Fig. 8 for SNR of -1 dB, 0 dB and 1 dB, while having only 2 tapers, 2 eigen channels and 16 carriers for the purpose of keeping simplicity in illustrations. The performance gains are quite apparent by leveraging larger SNR values, as it is typically expected in a wide range of communication systems. Generally, the most discernable feature perceived in the above figures is that the ROC trends have sharp climbing tendencies due to the incremental orders of the detector design parameters, precluding the FFT order of OFDM. Such featured trends demonstrate preferable conceptual performance stemmed from the vivid mixture of the space and signaling structures illustrated above.

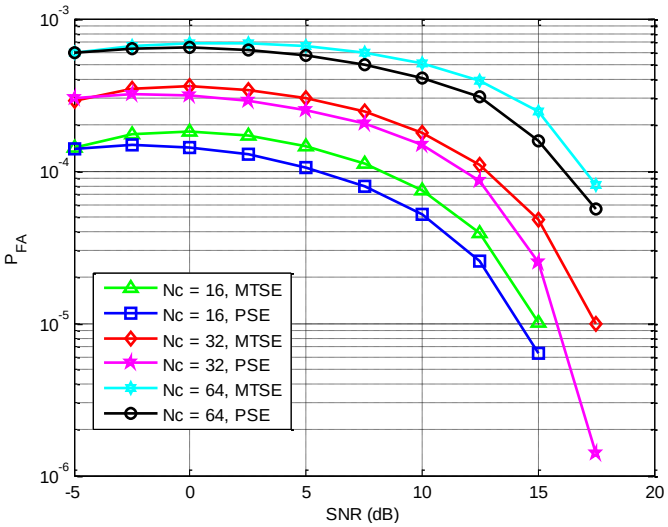

Fig. 9 P_{FA} of MTSE and PSE with 3 tapers and 2×2 MIMO versus SNR and OFDM variations.

The last simulation scenario is about a BPSK complex sequence of 128 data points admitted to 2×2 antennas channel of Rayleigh fading and immersed in AWGN impairments. The number of dominant tapers is set to be 3 and the sampling frequency of 1 MHz. Choosing a threshold value is challenging and occasionally can be fixed by trial and error; its value is adjusted to achieve the CFAR level of 10^{-3}, or better, in this exercise. The MTM has been compared to another non-parametric SE technique called the Periodogram (henceforth termed PSE). The FFT order of OFDM is varied in the range 16, 32, and 64. A Monte Carlo of 10^5 repetitions is considered and the performance improvements in the MTSE are obvious with respect to PSE, especially when the values of SNR increase dramatically beyond -5 dB as shown in Fig.9. However, inferior performance is obvious in both techniques with respect to the increase in the FFT order of OFDM. The higher the FFT order, or alternatively the number of carriers, the worse P_{FA} is obtained, which resembles the same result as in the ROC graphs earlier in this respect (see Figs. 5 and 6). Generally, the simulations confirm that the MTSE has better detection performance compared to the PSE under the same simulation settings. That is of course is credited to the powerful control of spectrum leakage exercised by the Slepian tapers in the MTSE compared to the normal rectangular windowing in the PSE approach. Special windowing techniques can also be exploited, such as Bartlett's method and Welch's method [6, 12, 13], however, the performance gain will be applicable to both MTSE and PSE and hence the MTSE outperformance sustains [13].

VII. Conclusion

This paper has investigated the foundation of SE approach using the non-parametric MTM scheme based on MIMO-OFDM transmission over AWGN and Rayleigh fading channels. The prime intention is to get around the viability of using the MTSE in sensing PUs' activities and provide with approximate asymptotes for the underlying detection probabilities. The main idea behind such an application is to seek improvements in detecting PUs' activities and fill in their licensed frequency holes if they are absent. The MTSE with few vital tapers, such as $L = 3$ as given in Fig. 9, shows very promising results in achieving better probability metrics in comparison to the classical PSE method. The more antennas, sequence samples and also M-ary size, the better performance can be realized. The contribution of prevailing MIMO and MRC techniques revealed added features towards further performance enhancements. While on the other hand, the OFDM transmission shows inferior detection trend in case the underlying FFT order increases. Therefore, special care is to be needed while trying to detect OFDM signals with large orders. This finding is in agreement with the OFDM inferiority discussion highlighted in [7]. Despite the OFDM poses as an attractive transmission for CR systems to combat channel fading, however, OFDM-based systems suffer from severe mutual interference between the PU and the SU systems. Therefore a trade-off in selecting appropriate transmission parameters, such as the number of MIMO antennas, OFDM carriers, modest tapers if the MTM is adopted for reception and alike, is always advisable. This is for the purpose to endeavor preferable channel performance while keeping an eye on efficient PUs' activities detection to facilitate opportunistic SUs. The merger of MTSE and MIMO technologies is envisaged to open wide doors for CR systems to arrive at resourceful management strategies aiming at better frequency spectrum utilization in future wireless systems.

References

[1] A. Ali and W. Hamouda (2017). Advances on spectrum sensing for cognitive radio networks: Theory and applications. IEEE Communications Surveys and Tutorials, 19(2): 1277-1303.

[2] B. Wang, K. Liu (2011). Advances in cognitive radio networks: a survey. IEEE J. of Selected Topics in Signal Processing. 5(1): 5-23.

[3] T. Yucek, H. Arslan (2009). A survey of spectrum sensing algorithms for cognitive radio applications. IEEE Communications Surveys and Tutorials. 11(1): 116-130.

[4] E. Axell, G. Leus, E. G. Larsson, H. V. Poor (2012). Spectrum sensing for cognitive radio: State-of-the-art and recent advances. IEEE Signal Processing Magazine. 101-116.

[5] S. Haykin, D. J. Thomson, J. H. Reed (2009). Spectrum sensing for cognitive radio. Proc. of the IEEE, 97(5): 849-877.

[6] S. Haykin (2005). Cognitive radio: Brain-empowered wireless communications. IEEE Trans. on Selected Areas in Communications, 23(2): 201-220.

[7] J. Ma, G. Y. Li and B. H. Juang (2009). Signal processing in cognitive radio. Proceedings of the IEEE. 97(5): 805-823.

[8] J. Wang, Q. T. Zhang (2009). A multitaper spectrum based detector for cognitive radio. Proc. Conf. Wireless Communications and Networks, Budapest, Hungary, pp 1-5.

[9] Q. Zhang (2011). Multitaper based spectrum sensing for cognitive radio: design and performance. Proc. Conf. Vehicular Technology, Yokohama, Japan, pp 1-5.

[10] M. K. Jataprolu, R. D. Koilpillai and S. Bhashyam (2012). Optimal MTM spectral estimation based detection for cognitive radio in HDTV. Proc. Nat. Conf. Communications, Kharagpur, India, pp 1-5.

[11] T. Yu, S. Parera, D. Markovic, D. Cabric (2010). Cognitive radio wideband spectrum sensing using multitap windowing and power detection with threshold adaptation. Proc Int. Conf. Communications, Cape Town, South Africa, pp 1-6.

[12] E. H. Gismalla, E. Alsusa (2012). New and accurate results on the performance of the multitaper-based detector. Proc. Int. Conf. Communications, Ottawa, Canada, pp 1609 – 1613.
[13] E. H. G. Yousif, T. Ratnarajah, M. Sellathurai (2015). Modelling and performance analysis of multitaper detection using phase-type distributions over MIMO fading channels. IEEE Trans. on Signal Processing, 63(22): 5882-5896.
[14] O. A. Alghamdi, M. A. Abu-Rgheff (2010). Local MTM-SVD based spectrum sensing in SIMO OFDM cognitive radio under bandwidth constraint. Proc. Int. Conf. Cognitive Radio Oriented Wireless Networks and Communications, Cannes, France, pp 1 - 6.
[15] G. L. Stuber, J. R. Barry, S. W. McLaughlin, Y. LI, M. A. Ingram, T. G. Pratt (2004). Broadband MIMO-OFDM wireless communications. Proc. of the IEEE, 92(2): 271-294.
[16] T. Hwang, C. Yang, G. Wu, S. Li, G. Y. Li (2009). OFDM and its wireless applications: a survey. IEEE Transactions on Vehicular Technology, 58(4): 1673-1694.
[17] H. A. Mahmoud, T. Yucek, H. Arslan (2009). OFDM for cognitive radio: merits and challenges. IEEE Wireless Communications: 6-14.
[18] A. Gupta, R. K. Jha (2015). A survey of 5G network: architecture and emerging technologies. IEEE Access, 3: 1206-1232.
[19] D. Brennan (2003). Linear diversity combining techniques. Proc. of the IEEE, 91(2): 331-356.
[20] B. Clerckx, C. Oestges (2013). MIMO wireless networks: channels, techniques and standards for multi-antenna, multi-user and multi-cell systems. Academic Press, 2013.
[21] A. Goldsmith (2005). Wireless communications. Cambridge University Press.
[22] S. Al-Juboori, X. Fernando (2015). Unified approach for performance analysis of cognitive radio spectrum sensing over correlated multipath fading channels. Proc. IEEE Int. Sym. World of Wireless, Mobile and Multimedia Networks, Boston, USA, pp 1-6.
[23] V. Kuppusamy, R. Mahapatra (2008). Primary user detection in OFDM based MIMO cognitive radio. Proc. Int. Conf. Cognitive Radio Oriented Wireless Networks and Communications, Singapore, pp 1-5.
[24] A. Nafkha, B. Aziz (2014). Closed-form approximation for the performance of finite sample-based energy detection using correlated receiving antennas. IEEE Wireless Communications Letters, 3(6): 577-580.
[25] N. Wang, Y. Gao (2013). Optimal threshold of Welch's periodogram for sensing OFDM signals at low SNR levels. Proc. Conf. European Wireless, Guildford, UK, pp 1-5.
[26] D. R. Joshi, D. C. Popescu, O. A. Dobre (2010). Dynamic threshold adaptation for spectrum sensing in cognitive radio systems. Proc. IEEE Radio and Wireless Symposium, New Orleans, USA, pp 468-471.
[27] S. M. Kay (1998). Fundamentals of statistical signal processing: detection theory Prentice-Hall PTR.
[28] Z. Quan, S. Cui, A. H. Sayed, H. V. Poor (2009). Optimal multiband joint detection for spectrum sensing in cognitive radio networks. IEEE Transactions on Signal Processing, 57(3): 1128-1140.
[29] T. E. Bogale, L. Vandendorpe, L. B. Le (2015). Wideband sensing and optimization for cognitive radio networks with noise variance uncertainty. IEEE Transactions on Communications, 63(4): 1091-1105.
[30] A. Taherpour, S. Gazor, M. N.-Kenari (2008). Wideband spectrum sensing in unknown white Gaussian noise. IET Communications, 2(6): 763-771.
[31] H. Qing, Y. Liu, G. Xie, J. Gao (2015). Wideband spectrum sensing for cognitive radios: A multistage Wiener filter perspective. IEEE Signal Processing Letters, 22(3): 332-335.
[32] T. Betlehem, A. J. Coulson, A. B. Reid (2010). Wide-band spectrum sensing for cognitive radio by combining antenna signals. Proc. Australian Communications Theory Workshop , Canberra, Australia, pp 111-116.